Comparative Evaluation of Virtual Inertia and Fast Frequency Reserve Provided by HVDC Terminals

Paula B. Garcia-Rosa
[1]SINTEF Energy Research
Trondheim, Norway
paula.garcia-rosa@sintef.no

Salvatore D'Arco
[1]SINTEF Energy Research
Trondheim, Norway
salvatore.darco@sintef.no

[1,2]Jon Are Suul
[2]Dept. of Engineering Cybernetics, NTNU
Trondheim, Norway
Jon.A.Suul@sintef.no

***Abstract*—This paper compares the impact on power system frequency transients from virtual inertia and Fast Frequency Reserve (FFR) provided by HVDC converters. Specifically, frequency nadir, Rate-of-Change-of-Frequency (RoCoF), and the required energy during the frequency support are evaluated. Two control schemes for providing virtual inertia are considered, including a current controlled Virtual Synchronous Machine (VSM) and a grid-following control with frequency derivative-based inertia emulation. The studied FFR provides either short or long support according to the guidelines of the Nordic synchronous area. Simulation studies are conducted in DIgSILENT PowerFactory using a 44-bus simplified model of the Nordic power system. With the same peak power, the results show that the different strategies have similar impact on the frequency nadir, while only the virtual inertia improves the RoCoF. Furthermore, the strategies for virtual inertia support can provide improvement of the frequency nadir with significantly less injected energy than the FFR long support.**

***Index Terms*—Fast Frequency Reserve, Frequency Nadir, Inertia Emulation, Rate-of-Change-of-Frequency, Virtual Inertia, Virtual Synchronous Machines**

I. Introduction

The ongoing transformation of the power system towards dominant shares of converter-interfaced generation is leading to declining equivalent inertia [1]–[3]. Thus, the power system research community and the Transmission System Operators (TSOs) are dedicating increasing efforts towards identifying and extending the limits for safe operation of power systems with low levels of physical inertia in terms of rotating mass directly connected to the grid [4]–[7].

To mitigate the effects of declining physical inertia, a wide range of control strategies have been proposed for utilizing power electronic converters to provide virtual inertia [8]–[12]. These control methods can generally be organized within two categories, depending on whether the implementation is based on "grid-following" or "grid-forming" control [13]. Specifically, virtual inertia provided by "grid-following" control relies on conventional grid synchronization strategies, for instance by a Phase Locked Loop (PLL), for introducing frequency-derivative-based Inertia Emulation (df/dt IE) as an auxiliary function [8], [14], [15]. Virtual inertia provided by "grid-forming" control strategies is instead based on explicit emulation of a virtual swing equation as part of a power-balance-based grid synchronization mechanism [9], [16], [17]. Thus, most "grid-forming" control strategies intended for providing virtual inertia can be considered to fall within the concept of Virtual Synchronous Machines (VSMs) [10]. However, fast frequency services such as Fast Frequency Reserve (FFR) are currently the main established mechanism for limiting frequency deviations in power systems [18], [19].

Power system support by FFR represents a fast active power provision that is available within a few seconds after a major disturbance. The profile of the provided power is usually not critical, but the grid codes specify requirements for the maximum activation time and the duration of support [19]. While FFR and strategies for providing virtual inertia have similar purposes in terms of limiting the maximum frequency deviations of a power system, the mechanisms of operation are rather different. Thus, they have been typically studied in different contexts. For instance, most studies related to "grid-following" or "grid-forming" strategies for providing virtual inertia have focused on the controller design and the performances of individual units. In contrast, studies related to FFR have been mainly related to power system operational aspects. The differences in focus are also amplified by the contrast between the many possible schemes for virtual inertia control and the simplicity of implementation for FFR. Indeed, the FFR specifications in [19] imply a direct power injection that does not significantly depend on the local control of the unit providing the service.

A comparative discussion of synthetic (or virtual) inertia versus fast frequency response was presented in [18]. This study defined synthetic inertia control to be a frequency-derivative effect, without considering the combination with a frequency droop. Furthermore, the evaluated control for fast frequency response was based on a droop control and not a power injection according to the recently introduced specifications for FFR services. Considering the increasing penetration of wind power generation as an example, the differences in impact on the frequency dynamics from the the virtual inertia and the droop control were discussed. It was also highlighted that the pure virtual inertia control will not improve the frequency regulation during normal operation. A further comparison

This work was supported by the project "HVDC Inertia Provision (HVDC Pro)", funded by the Research Council of Norway's ENERGIX Program under Project 268053/E20, and industry partners, Statnett, Equinor, RTE, and ELIA.

978-1-6654-6738-4/22/$31.00 ©2022 IEEE

This is the accepted version of an article published in 2022 14th IEEE PES Asia Pacific Power & Energy Engineering Conference - APPEEC

between virtual inertia and "fast" Frequency Containment Reserves (FCRs) was performed in [20], [21] by employing either batteries or electric vehicles as energy sources. However, the studied "fast" FCR included only a droop, in a similar way as the example of fast frequency response implemented in [18]. Thus, the impact on the frequency transients from the operating principle of the FFR according to the grid code specifications, i.e., acting mainly as a constant power injection during a few seconds after major disturbances, has not been addressed in these studies.

Considering the limitations of existing literature, a comparative evaluation of different methods for virtual inertia control and FFR provision by utilizing HVDC terminals is presented in this paper. For this purpose, a simplified 44-bus model of the Nordic power system [22], simulated in DigSILENT Power Factory, is applied as a test case. A reference condition is established by simulating a large load transient without considering any FFR or virtual inertia control. Then, four cases with virtual inertia or FFR support are simulated. These include the df/dt-IE as an example of a grid-following strategy for providing virtual inertia, a Current Controlled (CC)VSM as an example of a "grid-forming" strategy for providing virtual inertia, and FFR with short (5 s) or long (30 s) duration according to the specifications of the Nordic synchronous area. The time domain response for the five conditions are compared to evaluate how the fast frequency support influences the frequency nadir, the Rate-of-Change-of-Frequency (RoCoF), and the energy required for providing the frequency support. The results confirm how the different strategies for inertia emulation and the FFR have a similar impact on the frequency nadir as long as the peak injected power is the same. However, the FFR cannot influence the maximum RoCoF value, which occurs before reaching the frequency levels where the FFR is activated. Furthermore, the results show that the virtual inertia control can provide the same improvement of the nadir as the FFR with less required energy than the FFR long support in the initial 30 seconds after the disturbance.

II. Control of HVDC converters for frequency support

A. *Conventional Control with Fast Frequency Reserve support*

This work considers an FFR contribution according to the specifications defined for the Nordic power system [19], [23]. In this case, the FFR responds with a fast active power support to specific frequency deviations. The Nordic synchronous area operates at a nominal grid frequency of 50 Hz. In the event of major imbalances between active power generation and consumption, the frequency should not drop below 49 Hz. The FFR complements the upwards Frequency Containment Reserve for Disturbances (FCR-D) to secure frequency stability when the system kinetic inertia is low [23].

Table I indicates the frequency activation levels and the corresponding maximum activation time (t_a) for the FFR. In addition, short and long support duration are considered, as illustrated in Fig. 1. In the short support duration, the

TABLE I
FFR activation requirements in the Nordic power system [23].

Alternative	Activation level [Hz]	t_a [s]
A	49.7	1.3
B	49.6	1.0
C	49.5	0.7

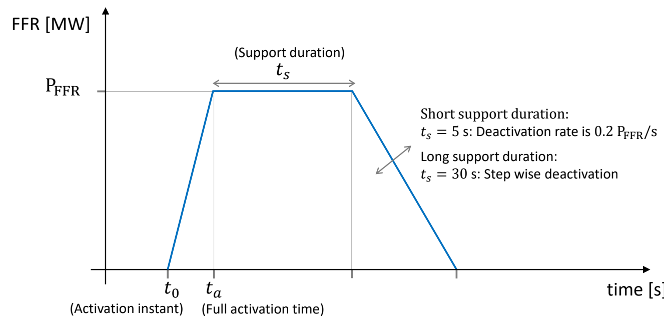

Fig. 1. Basic FFR definitions in the Nordic power system.

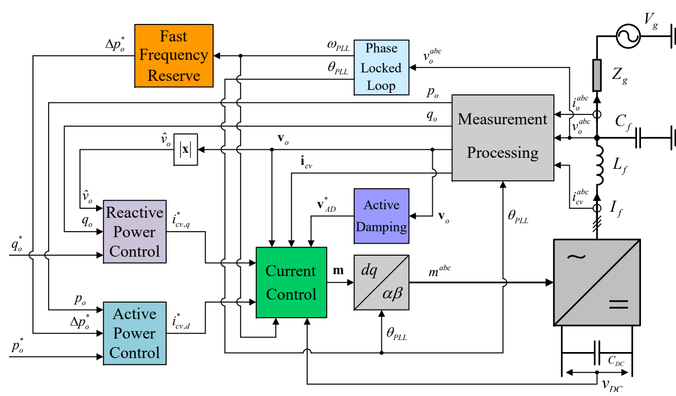

Fig. 2. Conventional converter control with additional power reference provided by the FFR.

active power support should last at least 5 s and the rate of deactivation is limited to maximum 20% of the FFR provision per second. In the long support duration, the support is for at least 30 s and the deactivation can be stepwise [23].

In this work, the FFR is provided through HVDC converters by including an additional power reference in a conventional PLL-based control structure. Fig. 2 shows an overview of the control system consisting of inner loop current controllers and closed loop control of active and reactive power. When the frequency estimated by the PLL (ω_{PLL}) reaches one of the activation levels in Table I, the additional power reference (Δp_o^*) follows the shape illustrated in Fig. 1.

B. *Conventional Control with df/dt Inertia Emulation*

Similar to the FFR scheme used in this work (Fig. 2), the df/dt IE scheme is also based on calculating an additional power reference for the power electronic converter. The converter control is the same conventional control scheme as for the FFR, but with the FFR block of Fig. 2 replaced

This is the accepted version of an article published in 2022 14th IEEE PES Asia Pacific Power & Energy Engineering Conference - APPEEC

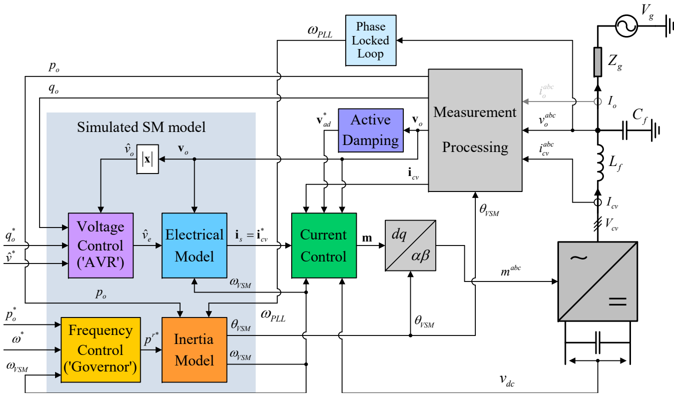

Fig. 3. Overview of the CCVSM (QSEM) control structure [24].

by the calculation of the equivalent inertial response of a synchronous machine. This includes the frequency reference ω^* as an additional input to the block. Then, the additional power reference is calculated as [14], [15]:

$$\Delta p_o^*(s) = -k_J \frac{s\omega_{LPF}}{s+\omega_{LPF}} \omega_{PLL}(s) + k_\omega(\omega^*(s) - \omega_{PLL}(s)) , \quad (1)$$

where the first term represents the filtered derivative of the grid frequency estimated by the PLL, and the second term is a frequency droop. The filtered derivative ensures that the transfer function is proper and attenuates high frequency noise. In (1), ω_{LPF} is the crossover frequency of the low-pass filter, k_J is the constant associated with the equivalent inertia, and k_ω is the frequency droop gain.

C. Current Controlled Virtual Synchronous Machine (VSM)

A third case considered in this work is a CCVSM with a Quasi-Stationary Electrical Model (QSEM) for implementing a virtual impedance. This scheme has been labelled as a CCVSM QSEM, and an overview of the control structure is shown in Fig. 3 [24]. The dynamic behavior of the virtual rotor position is defined by a simulated swing equation model as:

$$s\,\omega_{VSM}(s) = \frac{p^{r*}(s)}{T_a} - \frac{p_o(s)}{T_a} - k_d\frac{\omega_{VSM}(s) - \omega_{PLL}(s)}{T_a} \quad (2)$$

$$s\,\delta_{VSM}(s) = \omega_{VSM}(s) , \quad (3)$$

where ω_{VSM} and δ_{VSM} are the virtual rotor speed and position. Moreover, p_o is the output power from the converter, k_d is a damping coefficient, and T_a is the inertia time constant. This model ensures a power-balance-based grid synchronization mechanism and provides the virtual rotor position that is utilized in the Park transformation instead of the voltage phase angle from a PLL.

A frequency droop is introduced in the virtual power input to the simulated swing equation, to mimic the steady-state operation of a governor in a synchronous generator. The droop effect is defined by:

$$p^{r*}(s) = p_o^*(s) + k_\omega\,(\omega^*(s) - \omega_{VSM}(s)) , \quad (4)$$

where k_ω has the same function as for the df/dt IE. Furthermore, the references for the current controller are obtained by the QSEM implementation of the virtual impedance, as:

$$\boldsymbol{i}_{cv}^*(s) = \frac{\hat{v}_e(s) - \boldsymbol{v}_m(s)}{r + j\,\omega\, l} , \quad (5)$$

where r and l are the resistance and inductance of the virtual impedance. The variables $\boldsymbol{v}_m$ and $\hat{v}_e$ represent the filtered dq voltage components measured on the converter terminal and the amplitude of the induced voltage on the virtual stator windings, respectively.

III. Numerical Simulations

This section presents a comparison of the effects of virtual inertia and FFR on the transient behaviour of the grid frequency, and the additional energy supplied by the HVDC converter terminal providing the fast frequency support.

A. Power network and simulation parameters

The numerical simulations employ the Nordic 44-bus (N44) model [22], which is a simplified representation of the Nordic synchronous area. Fig. 4 shows the single-line diagram of the model, as implemented in DIgSILENT PowerFactory. More details about the N44 model and how the inertia and governor of the generators were calibrated for this work can be found in [25]. In the simulation model, only the primary control is implemented, which corresponds to the actuation of frequency containment reserves.

The simulations consider nine HVDC interconnections modelled as loads, except for the link providing frequency support. In this case, the parameters of the controlled terminal represent the bipolar HVDC Nordlink, which has rated capacity of 1500 MVA $\pm$ 525 kV dc, and is implemented as described in [26]. The converters are connected to the N44 model through grid-side filters and transformers in one side. In the other side, the converters are connected to an equivalent ac voltage source, which represents a simplified strong grid. The main parameters of the HVDC link, including FFR, df/dt IE and VSM-based control schemes, are listed in Table II.

B. Simulation results

The simulation results present two case studies with a disconnection of production units at bus 5300, in Norway, corresponding to a loss of about 2500 MW after 5 seconds of simulation. In Case Study 1 (CS1), fast frequency support is provided by one HVDC interconnection at bus 5620, while in Case Study 2 (CS2), the support is provided by two HVDC interconnections, at buses 5620 and 6000.

Fig. 5 shows a comparison of the CS1 results for the initial system without frequency support from the HVDC converter, and for the system when the HVDC converter control implements the CCVSM with QSEM, df/dt IE, FFR short support, and FFR long support. The results show the frequency of the generator at bus 5400 (G5400), the centre of inertia (COI) frequency, the output power from the converter negative terminal, and the mechanical power at the generator G5400. Fig. 6 presents a zoom of the initial transient for 30 s after the disturbance, which is the relevant time-window for

This is the accepted version of an article published in 2022 14th IEEE PES Asia Pacific Power & Energy Engineering Conference - APPEEC

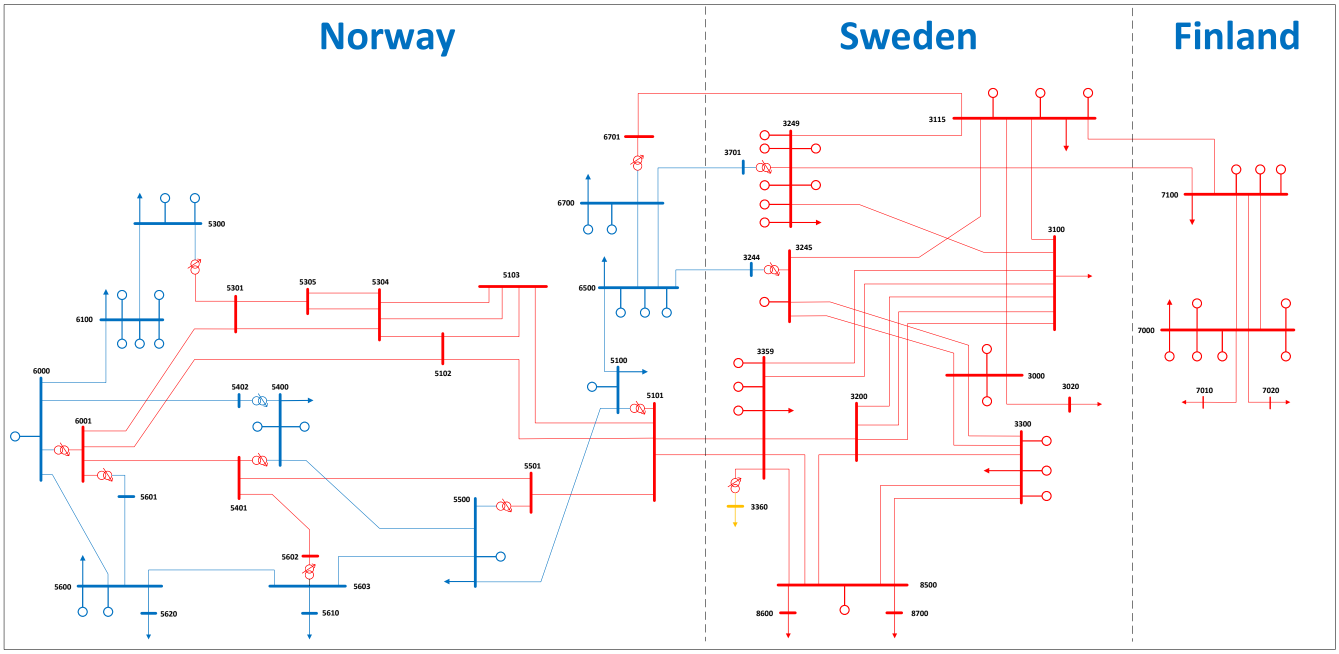

Fig. 4. Single-line diagram of the Nordic 44-bus model.

TABLE II
MAIN SIMULATION PARAMETERS HVDC AND FREQUENCY SUPPORT SCHEMES.

Parameter	Value	Parameter	Value
Rated ac voltage	285 kV	Rated grid frequency	50 Hz
Frequency droop gain (k_ω)	20 pu	Filter capacitance	0.074 pu
VSM damping factor (k_d)	75 pu	Filter inductance	0.08 pu
VSM inertia constant (T_a)	5 s	Filter resistance	0.003 pu
df/dt IE k_J constant	10	FFR activation level	49.7 Hz
df/dt IE crossover frequency (ω_{LPF})	0.16 rad/s	FFR short/ long support duration (t_s)	5 s/ 30 s

TABLE III
FREQUENCY NADIR AND MAXIMUM ROCOF AFTER THE UNIT TRIPPING.

Type of support	Nadir (Hz)		RoCoF (Hz/s)	
	CS1	CS2	CS1	CS2
Initial system	48.70	48.70	0.80	0.80
CCVSM (QSEM)	49.02	49.20	0.73	0.68
df/dt IE	49.03	49.21	0.71	0.64
FFR short	49.00	49.10	0.80	0.80
FFR long	49.02	49.20	0.80	0.80

fast frequency support provided by FFR. Notice that to make a fair comparison of the methods, the VSM- and df/dt IE-based control strategies are tuned to provide the same peak power as the reference power for the FFR support (Fig. 5.c).

In the simulation results, the FFR results in a small overshoot for both types of support (short and long), while the virtual inertia schemes provide a more damped response, which depends on the tuning of parameters (Fig. 5.a and Fig. 5.b). For all the cases with fast frequency support from the HVDC converter, the frequency nadir is improved when compared to the initial system. However, the RoCoF is only improved for the virtual inertia schemes, as the activation instant of the FFR support is about 1.5 s after the incident, i.e. when the frequency passes the threshold value of 49.7 Hz. Table III summarizes the obtained results of nadir and maximum RoCoF (over a window of 500 ms) for both case studies. It can be seen that the FFR short support duration results in a slightly lower nadir, as the power is reduced before the frequency starts to rise again (Fig. 6.c). In addition, the peak power at G5400 is higher during the initial transient, when the FFR short support is implemented (Fig. 6.d).

Fig. 5.b shows that the frequency does not reach the nominal value of 50 Hz in steady-state, as the secondary control, or Frequency Restoration Reserve (FRR), is not implemented. Due to the steady-state error in the frequency, the droop term included in the virtual inertia schemes (VSM and df/dt IE) prevents the power injected by the converter from returning to the initial condition, i.e. zero in this case. In the real system, the FRRs should be activated within 30 seconds after the incident to restore the frequency to the nominal value, and to release the FCRs. This would gradually return the power injection to the initial condition, according to the regular set-points for the HVDC transmission.

Fig. 7 compares the energy (W_o) provided by the converter(s) for both case studies. For the initial 10 s after the incident, the energy is nearly the same for all the fast frequency support schemes. However, within the time-window of 30 s after the incident, the FFR short support required about 75% less energy than the long support and about 50% less than the virtual inertia schemes. Furthermore, the virtual inertia control required about 50% less energy than the FFR long support.

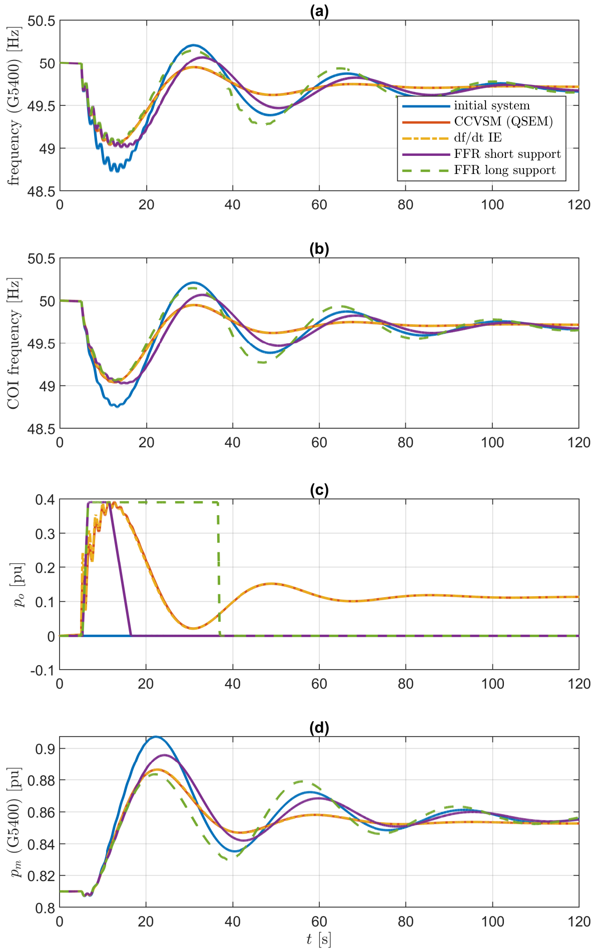

Fig. 5. CS1 simulation results: Full time-series of (a) frequency at G5400, (b) COI frequency, (c) output power from the converter negative terminal, (d) mechanical power at G5400.

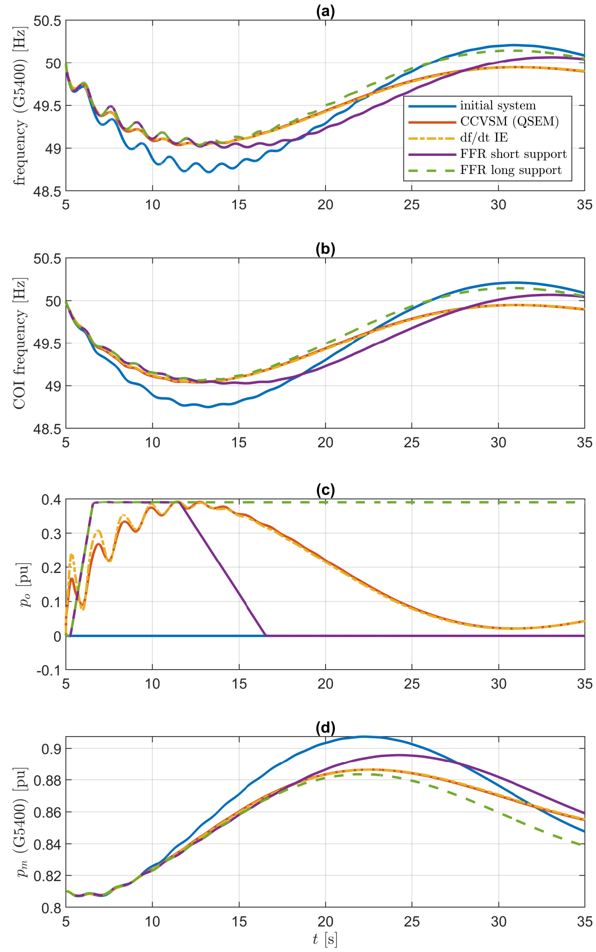

Fig. 6. CS1 simulation results: Zoom in transient period from 5 to 35 s: (a) frequency at G5400, (b) COI frequency, (c) output power from the converter negative terminal, (d) mechanical power at G5400.

C. Discussion

Virtual inertia and FFR services provide fast frequency support to help alleviate the challenges of low inertia power systems. However, the types of support are conceptually different. Indeed, virtual inertia control mimics the inertial response of synchronous generators, which can be naturally combined with a droop response as in traditional power plants, and provides a power response that follows the frequency dynamics immediately after a frequency deviation. Instead, the FFR provides a constant power response during a few seconds after a major disturbance. This work considers the current FFR regulations from the Nordic synchronous area. In other countries, e.g., in Ireland, the new fast frequency response service requires a sustainable power response for at least 8 seconds within 2 seconds after an incident [27].

The main drawback of delaying the response to a power imbalance is that the maximum RoCoF after the disturbance is not affected. In the Nordic system, the RoCoF is not a critical aspect, as the reference incident of the system did not involve high RoCoF values [28]. However, low inertia conditions and the disturbance location might result in a different scenario.

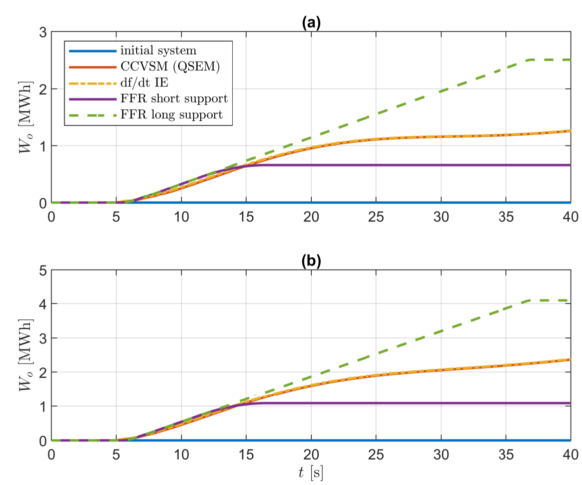

Fig. 7. Energy required during the frequency support through the HVDC converter(s): (a) CS1, (b) CS2.

This is the accepted version of an article published in 2022 14th IEEE PES Asia Pacific Power & Energy Engineering Conference - APPEEC

The presented simulation results indicate that the considered frequency support mechanisms provide similar impact on the frequency nadir. However, the FFR short support (5 s of duration) results in slightly lower values, as the deactivation starts before the nadir is reached. This effect might become more evident when a large number of converters are controlled for fast frequency support purposes. While this effect does not occur with the FFR long duration support, the energy used in this case is much higher. In contrast, virtual inertia control including a frequency droop results in a power response that inherently follows the dynamics of the frequency. Furthermore, for the compared metrics, no significant differences were observed between virtual inertia support by "grid-following" or "grid-forming" control schemes.

IV. Conclusion

The simulation results presented in this paper indicate how both virtual inertia control and FFR can mitigate the power imbalance in response to a sudden loss of generation. Thus, both approaches for fast frequency support help to stabilise the system frequency at acceptable values. However, the FFR does not inherently reduce the maximum RoCoF since the active power is injected more than 0.5 s after the disturbance has occurred. Furthermore, virtual inertia control provides a more damped response, as it naturally follows the frequency dynamics of the power system. The results also show how the frequency nadir is less sensitive than the RoCoF to how the active power is provided; the support by FFR long duration or by virtual inertia results in the same frequency nadir. The FFR short duration results in slightly lower values because the power injection is deactivated before the frequency has reached the minimum value. For the initial transient within 30 seconds after the disturbance, the FFR long support requires about twice the energy of what is required by the virtual inertia schemes and four times what is required by the FFR short support duration. Thus, virtual inertia control combined with frequency droop can provide fast frequency support to improve the nadir with less required energy than FFR long support, with the additional benefit of improving the RoCoF.

References

[1] Y. Wang, V. Silva, and M. Lopez-Botet-Zulueta, "Impact of high penetration of variable renewable generation on frequency dynamics in the continental europe interconnected system," *IET Renewable Power Generation*, vol. 10, no. 1, pp. 10–16, 2016.

[2] B. Hartmann, I. Vokony, and I. Táczi, "Effects of decreasing synchronous inertia on power system dynamics – Overview of recent experiences and marketisation of services," *Int. Trans. on Electrical Energy Systems*, vol. 29, no. 12, p. e12128, 2019.

[3] L. Mehigan, D. Al Kez, S. Collins, A. Foley, B. Ó'Gallachóir, and P. Deane, "Renewables in the european power system and the impact on system rotational inertia," *Energy*, vol. 203, p. 117776, 2020.

[4] J. O'Sullivan, A. Rogers, D. Flynn, P. Smith, A. Mullane, and M. O'Malley, "Studying the maximum instantaneous non-synchronous generation in an island system–Frequency stability challenges in Ireland," *IEEE Trans. on Power Systems*, vol. 29, no. 6, pp. 2943–2951, 2014.

[5] M. Yu, A. J. Roscoe, A. Dyśko, C. D. Booth, R. Ierna, J. Zhu, and H. Urdal, "Instantaneous penetration level limits of non-synchronous devices in the British power system," *IET Renewable Power Generation*, vol. 11, no. 8, pp. 1211–1217, 2016.

[6] M. N. H. Shazon, A. Jawad *et al.*, "Frequency control challenges and potential countermeasures in future low-inertia power systems: A review," *Energy Reports*, vol. 8, pp. 6191–6219, 2022.

[7] J. Fang, H. Li, Y. Tang, and F. Blaabjerg, "On the inertia of future more-electronics power systems," *IEEE Journal of Emerging and Selected Topics in Power Electron.*, vol. 7, no. 4, pp. 2130–2146, 2018.

[8] J. Morren, S. W. De Haan, W. L. Kling, and J. Ferreira, "Wind turbines emulating inertia and supporting primary frequency control," *IEEE Trans. on Power System*, vol. 21, no. 1, pp. 433–434, 2006.

[9] H.-P. Beck and R. Hesse, "Virtual synchronous machine," in *Proc. of the 9th Int. Conf. on Electrical Power Quality and Utilisation*, 2007.

[10] S. D'Arco and J. A. Suul, "Virtual synchronous machines - Classification of implementations and analysis of equivalence to droop controllers for microgrids," in *Proc. of the IEEE Grenoble Conf.*, 2013.

[11] H. A. Alsiraji and R. El-Shatshat, "Comprehensive assessment of virtual synchronous machine based voltage source converter controllers," *IET Generation, Transmission & Distribution*, vol. 11, no. 7, pp. 1762–1769, 2017.

[12] S. Chen, H. Han, X. Chen, Y. Sun, and X. Hou, "Reviews on inertia emulation technology with power electronics," in *2020 IEEE Energy Conversion Congress and Exposition (ECCE)*, 2020, pp. 2101–2107.

[13] J. Rocabert, A. Luna, F. Blaabjerg, and P. Rodriguez, "Control of power converters in ac microgrids," *IEEE Trans. on Power Electronics*, vol. 27, no. 11, pp. 4734–4749, 2012.

[14] E. Rakhshani and P. Rodriguez, "Inertia emulation in ac/dc interconnected power systems using derivative technique considering frequency measurement effects," *IEEE Trans. on Power Systems*, vol. 32, no. 5, pp. 3338–3351, 2016.

[15] D. Duckwitz and B. Fischer, "Modeling and design of df/dt-based inertia control for power converters," *IEEE Journal of Emerging and Selected Topics in Power Electron.*, vol. 5, no. 4, pp. 1553–1564, 2017.

[16] Q.-C. Zhong and G. Weiss, "Synchronverters: Inverters that mimic synchronous generators," *IEEE Trans. on Industrial Electronics*, vol. 58, no. 4, pp. 1259–1267, 2010.

[17] M. Guan, W. Pan, J. Zhang, Q. Hao, J. Cheng, and X. Zheng, "Synchronous generator emulation control strategy for voltage source converter (VSC) stations," *IEEE Trans. on Power Systems*, vol. 30, no. 6, pp. 3093–3101, 2015.

[18] R. Eriksson, N. Modig, and K. Elkington, "Synthetic inertia versus fast frequency response: a definition," *IET Renewable Power Generation*, vol. 12, no. 5, pp. 507–514, 2018.

[19] ENTSO-E, "Technical requirements for fast frequency reserve provision in the Nordic synchronous area – External document. Version 1.1, Published 11 January 2021," *ENTSO-E, Tech. Rep.*, 2021.

[20] M. Rezkalla, M. Marinelli, M. Pertl, and K. Heussen, "Trade-off analysis of virtual inertia and fast primary frequency control during frequency transients in a converter dominated network," in *2016 IEEE Innovative Smart Grid Technologies - Asia (ISGT-Asia)*, 2016, pp. 890–895.

[21] M. Rezkalla, A. Zecchino, S. Martinenas, A. M. Prostejovsky, and M. Marinelli, "Comparison between synthetic inertia and fast frequency containment control based on single phase evs in a microgrid," *Applied Energy*, vol. 210, pp. 764–775, 2018.

[22] S. H. Jakobsen, L. Kalemba, and E. H. Solvang, "The Nordic 44 test network," *figshare*, 2018, https://doi.org/10.6084/m9.figshare.7464386.v1.

[23] N. Modig et al., "FFR design of requirements – External document Version 1.0," *ENTSO-E, Tech. Rep.*, 2020.

[24] O. Mo, S. D'Arco, and J. A. Suul, "Evaluation of virtual synchronous machines with dynamic or quasi-stationary machine models," *IEEE Tran. on Industrial Electronics*, vol. 64, no. 7, pp. 5952–5962, 2017.

[25] P. B. Garcia-Rosa, S. D'Arco, and J. A. Suul, "Placement of virtual inertia from HVDC terminals based on a frequency deviation index," in *2021 IEEE Madrid PowerTech*, 2021.

[26] F. Palombi, L. Piegari, S. D'Arco, A. G. Endegnanew, and J. A. Suul, "Impact on power system frequency dynamics from an HVDC transmission system with converter stations controlled as virtual synchronous machines," in *Proc. of IEEE Milan PowerTech*, 2019.

[27] EirGrid Group, "System services test report. Fast Frequency Response (FFR), Primary, Secondary and Tertiary Reserve (POR, SOR, TOR1, TOR2); Aggregators. Template Version 4.0, Published 21 March 2020," *EirGrid, SONI, Test Rep. Template*, 2020.

[28] Nordic Analysis Group, NAG, "Requirement for minimum inertia in the Nordic power system," *ENTSO-E, Tech. Rep.*, 2021.

This is the accepted version of an article published in 2022 14th IEEE PES Asia Pacific Power & Energy Engineering Conference - APPEEC